5 Particle Physics at DESY/HERA

S. Egli, S. Hengstmann, D. Müller, M. zur Nedden, P. Robmann, F. Sefkow,
P. Truöl, T. Walter,
in collaboration with
M. Biddulph, R. Eichler, J. Gassner, C. Grab, M. Hilgers, H.-C. Kästli,
S. Lüders, U. Langenegger, H. Niggli, S. Passagio, D. Pitzl, and Y. Tsipolitis,
Institut für Teilchenphysik der ETH, Zürich
K. Gabathuler, and R. Horisberger
Paul–Scherrer–Institut, Villigen,
and 34 institutes outside Switzerland
(**H1**–Collaboration)

5.1 Electron proton collisions at 300 GeV center of mass energy: overall status of the project

The operation of the HERA accelerator complex has been continously improved in reliability as well as in peak performance. This is demonstrated by the luminosity curves in Figure 5.1 and the data collected in Table 5.1. The 1997 run was particularly successful, and exceeded the scheduled goals by a factor of 1.4. Though the maximum proton and positron currents reached only 76 % and 69 %, respectively, of their design values so far, peak luminosities in H1 with 67 % of the design value (15 $(\mu\mathrm{b\ s})^{-1}$) are found, because the beam dimensions ($179 \times 48\ \mu\mathrm{m}^2$) are twice smaller than predicted. For the magnet cycling, preaccelerator preparation, storage ring filling and energy ramping of the positron and proton ring to 27.5 GeV and 820 GeV, respectively at least three hours are needed, which is why the running efficiency (luminosity delivery divided by total time) is limited to 80 %. Technical failures, repairs and deficit in controls however limited the running efficiency to 42 %, a value which is continuously increasing, in particular if no long shutdowns interupt the schedule. We are presently at the end of such a long shutdown, in which among other technical improvements the vacuum system of the electron/positron ring was upgraded in order to increase the electron beam life time. Luminosity operation is going to resume only in August 1998, with electron acceleration as well as higher proton beam energies (up to 920 GeV) are foreseen.

With a total luminosity of 45 pb^{-1} now accumulated, the H1- as well as its rival ZEUS-collaboration have continued to explore the structure of the proton and scrutinize quantum chromodynamics predictions. The principal areas covered by recent and ongoing analyses are

- neutral and charged electroweak current cross sections [1],
- proton structure functions and parton densities in new domains of Bjorken x and momentum transfer Q^2 [1, 2, 3, 4],
- search for states outside the standard model [5],
- photoproduction at high invariant masses of the photon proton system and parton densities in the photon [6, 7, 8, 9],
- diffractive processes and the structure of the pomeron [10, 11, 12],
- testing perturbative and non-perturbative quantum chromodynamics predictions with the evolution of structure functions [2, 4],
- parton-fragmentation into exclusive and multijet final states [13, 14, 15, 16], and
- production of heavy quark-antiquark states [17, 18, 19, 20].

Though the luminosity is still insufficient to accumulate yet large event samples for the most important electroweak processes at high momentum transfer ($Q^2 \approx M_W^2$), our first paper

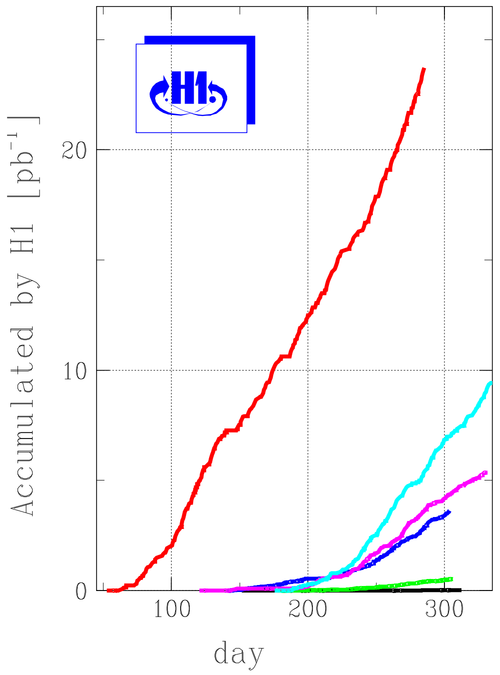

Figure 5.1: Integrated luminosity during the first six years of HERA operation, as seen by the H1-detector (lowest curve: 1992, highest curve: 1997).

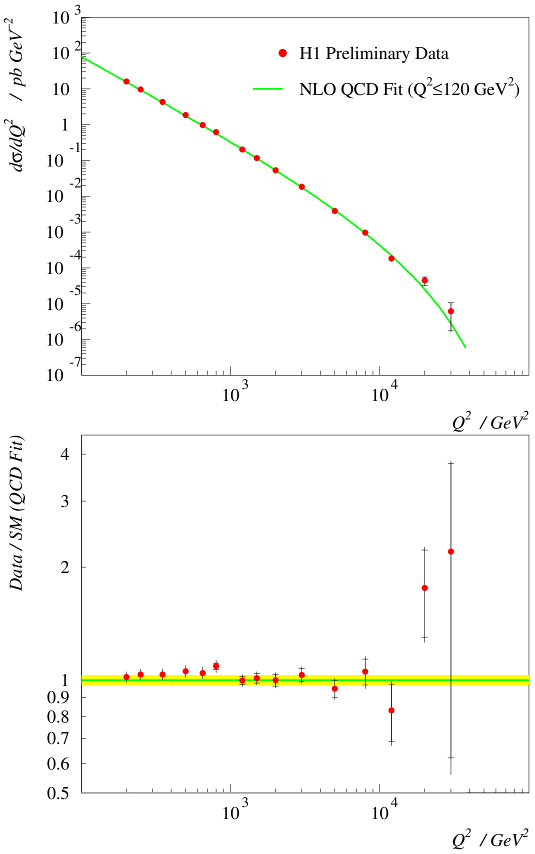

Figure 5.2: High-momentum transfer inclusive single differential cross section $d\sigma/dQ^2$ for deep inelastic positron proton scattering (top), and deviations of the data from the next-to-leading order QCD fit (bottom)

[1], which dealt with this region ($Q^2 > 15000$ GeV^2) led to a great deal of excitement, since the number of observed events exceeded that expected within the standard model description of deep inelastic lepton scattering. The data collected since then in 1997 do not show such an excess [3, 4], but at the highest accessible momentum transfers small differences still exist (see Figure 5.2 and Section 5.4.1).

To fully exploit the discovery potential of the HERA machine in the largely unexplored mass region near 200 GeV a luminosity upgrade is planned for the year 2000. Through a change of the beam focussing near the interaction region the luminosity will be increased by a factor of five. This is achieved by introducing new magnets within the H1 detector and requires modifications of its inner parts.

The activities of the University of Zürich group concern the maintenance, monitoring and continuous improving of the detector components built at Zürich for the central tracker and the first level trigger of H1, and participation in the physics analysis, in particular in the areas of photoproduction, charmed quark containing final states and deep inelastic scattering. As in the past we continued to be strongly involved in adapting the first level triggers to the increased beam currents and backgrounds at H1.

The construction of a new five-layer, central inner multiwire proportional chamber with finer granularity and increased redundancy will be a major contribution by the Zürich groups

Parameter	1992	1993	1994		1995	1996	1997
	e^-p	e^-p	e^-p	e^+p	e^+p	e^+p	e^+p
Integrated luminosity $\mathcal{L}$							
HERA produced [nb^{-1}]	–	999	938	5063	11437	14366	37574
HERA physics [nb^{-1}]	55	880	846	4743	10403	13299	35755
H1 taken [nb^{-1}]	30	568	532	3576	6414	8919	30434
H1 physics [nb^{-1}]	25	528	494	3489	5745	8648	26392
HERA efficiency [%]	–	88	90	94	91	92	95
H1 efficiency [%]	46	60	58	73	55	65	74
Average luminosity [(μb s)$^{-1}$]	0.03	0.27	0.62	1.29	2.13	2.64	4.38
Peak luminosity [(μb s)$^{-1}$]	0.22	1.3	2.6	4.3	5.9	8.4	10.1
Average p current [mA]	0.94	10.8	28.6	41.0	54.0	60.3	74.5
Average $e^{\pm}$ current [mA]	1.33	7.7	10.5	17.0	18.4	20.6	28.0
Colliding bunches	9	84	153	153	174	175	175
Pilot (e,p) bunches	1,1	10,6	15,17	15,17	15,6	14,6	14,6
HERA luminosity runs	132	218	116	176	304	241	411
Permanent H1 runs	1409	3190	1141	1816	4208	3582	5369
Average duration [s]	973	817	1115	1620	884	1159	1431

Table 5.1: Summary of HERA and H1 operation during the first six years.

to the upgrade of the H1-detector needed concurrent with the change of the interaction region.

5.2 Summary of activities related to the Zürich H1-components

During the shutdown 1997/8 the complete central and forward tracker was extracted from the H1 detector in order to rewire the central jet chamber, which showed degradation in the lower sectors. This gave us the opportunity to open both our central inner proportional chambers (CIP), measure the wire tensions (found unchanged) and search for radiation damage. Only in a small sector of one chamber, where full high voltage could no longer be reached, deposits were found. Five wires in this area were replaced and the chamber cleaned. Otherwise no radiation damage was apparent. The continuous monitoring of the chamber performance for the $z-$vertex trigger showed no degradation of the efficiency either. The central inner $z-$drift chamber (CIZ) was completely rewired, since radiation damage was observed in some of the fifteen rings, most prominently in those for which the wires were not replaced by new and especially cleaned ones previously. During 1997 the central silicon detector (CST) was fully operational. The fine tuning of the alignment parameters and the development of the reconstruction codes is nearly completed, with impact on the secondary vertex selection for the heavy quark analysis expected soon. During the shutdown 1997/8 a few ladders were exchanged and the adapter tube, a lightweight sandwich construction containing the CST power cables and cooling pipes and surrounding the backward silicon detector, was completely rebuilt.

While the vertex detector is important for the reconstruction of events containing charm quarks, the $z-$vertex and drift chamber track triggers built and serviced by us and our ETH-colleagues are essential for triggering these events, which are characterized by low transverse energy. Since both Zürich groups also participate strongly in the analysis of these events, they also played a central role in their collection, i. e. in the careful reoptimisation of the trigger set-up for the 97 data taking, using feedback from our own ongoing analyses. These tasks include the responsibility for the verification of the whole on- and off-line selection chain for open charm.

In this respect we have also investigated [21] trigger possibilities with signals from the central inner MWPC (CIP) alone. The study was motivated, on one hand, by the ever increasing demands on background rejection, which relies heavily on the existing $z-$vertex trigger and will continue to do so until the full commissioning of the system envisaged for the HERA luminosity upgrade. On the other hand, using real data samples – beam gas background events, charm and jet photoproduction physics events –, allowed us to study, without having to make assumptions on simulated background, the performance of a thin MWPC system, i. e. one without the lever arm provided by the combination with the outer MWPC. In this respect we considered a trigger logic similar to that of the proposed upgrade. The results support the proposal for the CIP and vertex trigger envisaged with the HERA high luminosity upgrade (see Section 5.3 below). We found that already with the present chamber, a careful analysis of the backward part allows to recognize upstream tracks and to achieve a substantially improved background rejection while keeping physics inefficiencies at the percent level. With a relatively simple hardware modification such a logic can be implemented. For the proposed CIP upgrade, with a finer $z-$segmentation and five radial layers, a much better track angle resolution and thus much more powerful background discrimination can be expected.

In the analysis we concentrated on the following aspects: calibration and efficiency monitoring of CIZ and CIP, monitoring the performance of the $z-$vertex and big ray trigger elements, optimization of the trigger settings for charm events, optimizing D^*-tagging codes and determining the charm photoproduction and deep inelastic electroproduction cross section, deriving the gluon distribution in the proton from these data (see Section 5.4.2 below), and investigating high p_T charged particle photoproduction and its relation to the photon structure functions.

5.3 Upgrade plans

In order to achieve higher luminosities and higher event rates for the rare processes at the limits of the kinematically accessible range it is planned to upgrade the HERA machine complex [22]. The most important aspect of this program is the improvement of the focussing properties near the interaction region, which calls for a new lattice with machine magnets inside the detectors and new types of septum magnets. The consequent beam squeeze will allow for a luminosity $\mathcal{L} = 7.4 \times 10^{31}$ cm^{-2}s^{-1}, a factor of seven compared to what is presently achieved (see Table 5.1).

Unfortunately this scheme will generate synchrotron radiation inside H1, it can no longer be stopped before the experiment as in the present setup. This has a big impact on the beam pipe and absorber design, and will also require rearranging the central (CST) and backward (BST) silicon trackers. For the CST the same silicon ladders will be used, but new end flanges and support are needed.

As part of the upgrade project we proposed to replace the CIZ and the CIP with a five plane cylindrical proportional chamber [23]. This proposal was primarily motivated by the demand for higher redundancy and safer operation in a higher level of synchrotron radiation background, the need to resolve CST ambiguities and the desire to have a robust determination of the interaction vertex with a tracker element at high initial rates. The new CIP can make a sufficiently accurate determination of the vertex position and the event timing and help us keeping, in combination with the calorimeter, the high Q^2 events at initial top luminosities of a new fill, when other trackers can not be turned on yet. The new chamber will also be used for an improvement of the z-vertex trigger. A drawing of the new five layer proportional chamber with a pad width of 9 mm in sixteen ϕ−sectors is shown in Figure 5.3.

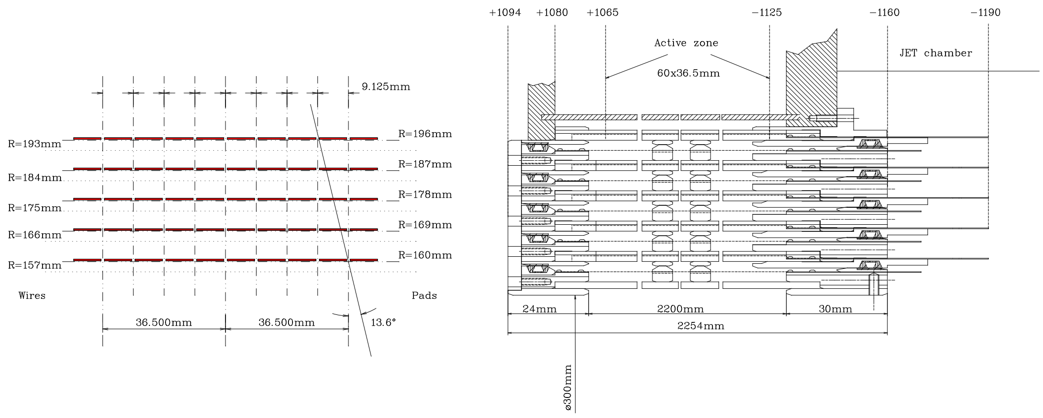

Figure 5.3: Cross section of the planned new central inner proportional chamber (right). Left: cathode pad structure (36.5 mm width in the present CIP).

5.4 Results from recent analyses

5.4.1 Deep inelastic scattering at highest momentum transfer and the standard model

The differential cross section for deep inelastic positron proton scattering may be written in terms of the two independent kinematical variables x and Q^2 as

$$\frac{d^2\sigma}{dx dQ^2} = \frac{2\pi\alpha^2}{xQ^4}\left[Y_+ F_2(x,Q^2) - y^2 F_L(x,Q^2) - Y_- xF_3(x,Q^2)\right] \ .$$

$Q^2(\equiv -t)$ is the squared four-momentum transfer of the scattered positron and x the fraction of the proton momentum carried by the struck quark. The variable y is defined as $y = Q^2/xs$, with s being the total positron-proton center of mass energy (300 GeV), and $Y_\pm(y)$ is defined as $Y_\pm = 1 \pm (1-y)^2$. F_2 and F_L are the generalized and the longitudinal structure function, respectively, F_3 is the parity violating term arising from Z_0 exchange. F_2 may be decomposed into three terms

$$F_2 = F_2^{em} + \frac{Q^2}{Q^2 + M_Z^2} F_2^{int} + \frac{Q^4}{(Q^2 + M_Z^2)^2} F_2^{weak} \equiv F_2^{em}(1 + \delta_Z)$$

F_2^{em} contains only photon exchange, F_2^{weak} only Z_0 exchange, and F_2^{int} the interference of both contributions. For convenience often the reduced cross section is used

$$\sigma(e^+p) \equiv \frac{xQ^4}{2\pi\alpha^2}\frac{1}{Y_+}\frac{d^2\sigma}{dx dQ^2} = F_2^{em}(1 + \delta_Z - \delta_3 - \delta_L) \ .$$

For the correction terms one finds $\delta_Z - \delta_3 < 1\%$ at $Q^2 < 1500$ GeV^2 and $\delta_Z - \delta_3 \approx 10\%$ at $Q^2 = 5000$ GeV^2 and $x = 0.08$, while δ_L is negligible at $y < 0.5$ and $\approx 5\%$ at $y = 0.9$. F_2 in turn is given by the sum of quark, antiquark and gluon densities.

Since both the positron and the final state hadrons marking the path of the struck quark are observed in the detector the kinematical variables can be reconstructed from angle and energy of either positron or hadronic jet or a combination of both. For example in terms of positron quantities one finds

$$y_e = 1 - \frac{E_e(1-\cos\theta_e)}{2E_e^0}\ , \qquad Q_e^2 = \frac{E_{T,e}^2}{1-y_e}\ , \qquad M_e = \sqrt{sx_e} = \sqrt{\frac{Q_e^2}{y_e}}\ .$$

M_e is the mass of the positron-quark system, $E_{T,e}$ the transverse energy of the positron, $E_e^0 = 27.5$ GeV and θ_e, the polar scattering angle measured from the proton direction. The H1-detector has good positron energy resolution, as evidenced by the calibration data displayed in Figure 5.4, which favors use of positron variables in particular at high momentum transfers, but important and quite accurate cross checks using the jet quantities are possible. These are important for charged current processes mediated by W exchange, where the kinematical quantities can only be deduced from the final state hadrons.

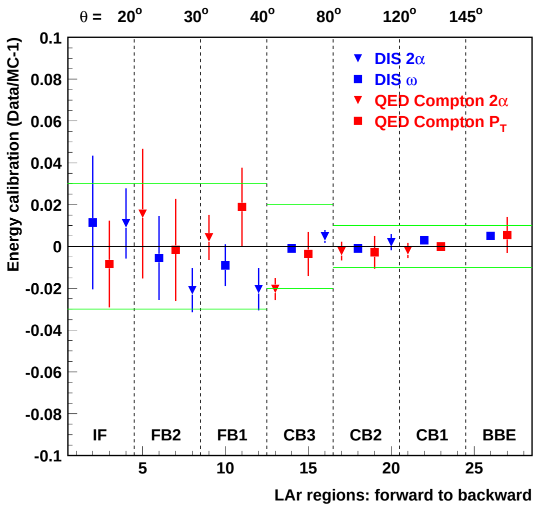

Figure 5.4: Present status of the liquid Argon electromagnetic calorimeter calibration. The data points are from reactions, where the electron or positron energy can be calculated from other kinematical quantities.

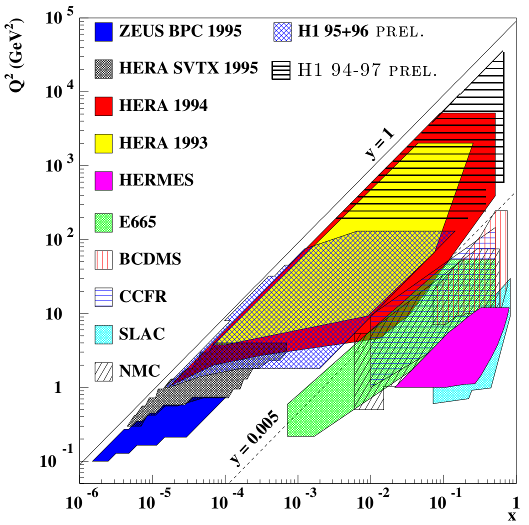

Figure 5.5: Regions covered by different experiments in the $(x, Q^2)-$plane. Entries with labels other than HERA, H1, or ZEUS are from fixed target experiments.

The high ep center of mass energy has meant that proton structure has been probed for the first time not only at high Q^2 but also at very low Bjorken x. In this kinematic region of low parton momenta the gluon density was found to be rising steeply (see e. g. [2]). Better understanding of all detector components, including the new components from the first upgrade in the analysis, has allowed to considerably extend the kinematical range (see Figure 5.5), also in the direction of high x where the gap to the lower Q^2 fixed target experiments could be bridged.

Displaying the integrated cross section $d\sigma/dQ^2$ as a function of Q^2, as done in Figure 5.2, is the most direct way to expose possible fermion substructure. Standard model predictions describe the data very well over seven orders of magnitude in cross section, nearly independent of how the parton densities are extrapolated from the low Q^2 data. Limits on fermion substructure can be set e. g. assuming a classical charge form factor

$$\frac{d\sigma}{dQ^2} = \left(\frac{d\sigma}{dQ^2}\right)_{SM} f_e(Q^2) f_q(Q^2) \quad \text{with} \quad f_{e/q} = 1 - \frac{1}{6}R_{e/q}^2 Q^2\ .$$

Since $(g-2)$ and (e^+, e^-) experiments already put stringent limits on the electron radius R_e the HERA data are sensitive to quark radii $R_q < 10^{-18}$ m.

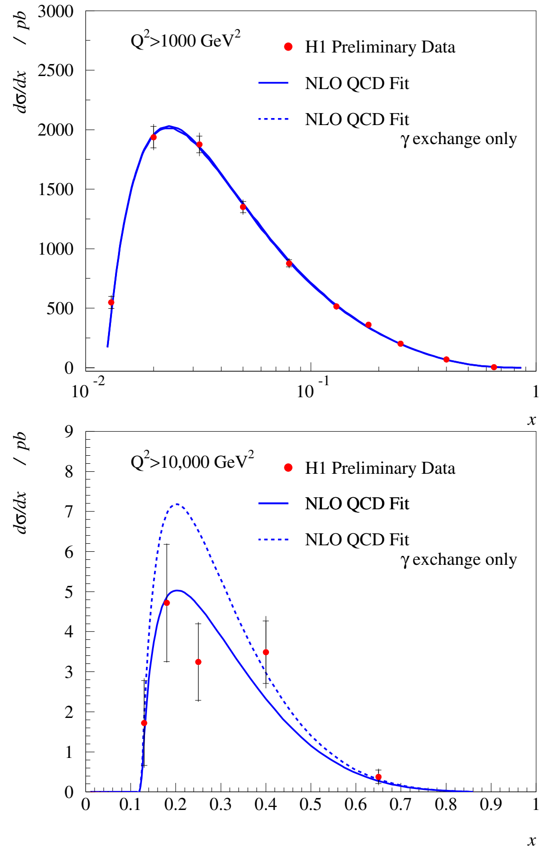

Figure 5.6: Differential cross section as function of x for $Q^2 > 1000$ GeV^2 and $Q^2 > 10000$ GeV^2 indicating the influence of the electroweak neutral current mediated by Z_0 exchange.

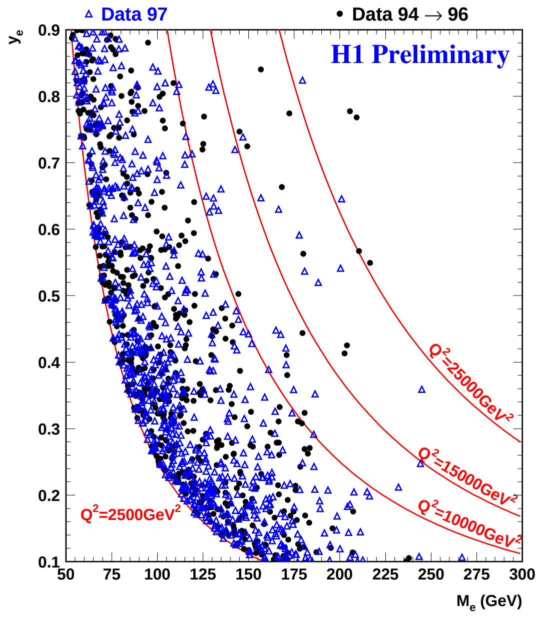

Figure 5.7: Distribution of events in the $(x, Q^2)-$plane. Filled circles: up to 1996 data (14.2 pb^{-1}), triangles: 1997 data (22.8 pb^{-1}). For $Q^2 > 5000$ GeV^2 322 events are observed, whereas 336±30 are expected, while for$Q^2 > 15000$ GeV^2 22 are found and 15±2 are expected.

Integrating the cross section over Q^2 above a certain high Q^2_{min} (see Figure 5.6) exhibits that one has to go to $Q^2_{min} = 10000$ GeV^2 to observe the influence of the valence quarks and of the Z_0 contributions, for $Q^2_{min} = 1000$ GeV^2 the cross section is still dominated by low x partons.

The small excess of events observed at the highest Q^2 (see Figure 5.2) was already present in the pre-1997 data sample comprising an integrated luminosity of 14.2 pb^{-1} [1]. Above $Q^2 = 5000$ GeV^2 144 events where found, while the the expectation from the standard neutral current deep inelatic scattering model was 136 ± 12, while above $Q^2 = 15000$ GeV^2 12 where found and 4.7 ± 0.8 expected, with a preference for a mass window of total width 25 GeV centered at an invariant mass $M_e \simeq 200$ GeV of the positron-parton system. Figure 5.7 shows the kinematical distribution of high Q^2 events in the (y, M_e) plane including the new events found in 1997 [3, 4]. The accumulated luminosity now is 37.0 pb^{-1}. The concentration of events in a given mass region is no longer observed, and the event count now yields for $Q^2 \geq 5000$ GeV^2 322 events (336 ± 30 expected) and for $Q^2 \geq 15000$ GeV^2 22 (15 ± 2). Thus the significance for the anomaly decreased last year. The corresponding charged current data ($ep \to \bar{\nu}_e X$) shown in Figure 5.9 lead to similar albeit statistically less significant conclusions.

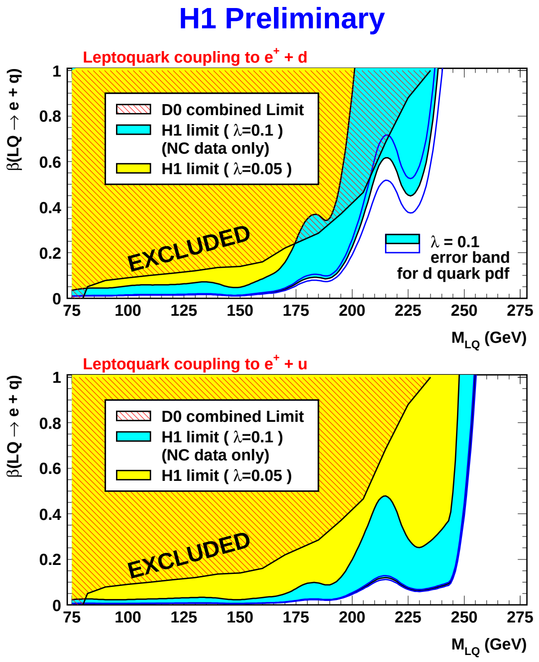

Figure 5.8: Limits for the branching ratio of a leptoquark decaying into a positron and a quark, assuming fixed values of the coupling constant λ versus the leptoquark mass (see [4]).

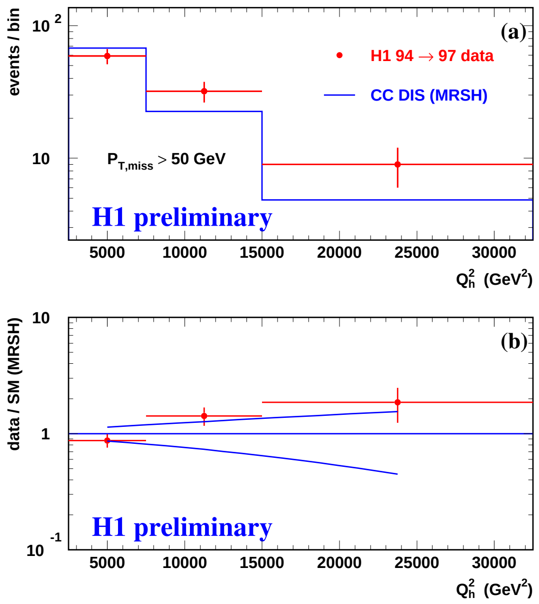

Figure 5.9: High Q^2 charged current data. The expected number of events (histogram) is compared to the number of events found. For $Q^2 > 2500$ (7500) [15000] 100 (41) [9] events are found, while 95$\pm$17 (28$\pm$8) [5$\pm$3] are expected (see [3] for details).

The data have also been analysed in order to limit the couplings and masses of hypothetical leptoquarks, postulated to exist in some extensions of the standard model. Competition in this area comes mainly from Fermilab-Tevatron experiments (e. g. $D0$).

Already in 1994 an event with unusual characteristics ($e^+p \to \mu^+X$) was observed in our detector. This event was found in the standard charged current analysis, showed an isolated high momentum muon recoiling against a system of hadrons and was unbalanced in momentum suggesting the presence of an undetected final state particle. This observation initiated a search for high energy isolated leptons in events which are unbalanced in transverse momentum in all the available data until now [5]. Five such events, four of them with isolated muons, one with an electron, were found within the about 500 charged current candidates with a missing transverse momentum exceeding 25 GeV. Only two of these events fit into a region of phase space, which is likely to be populated by W production followed by a leptonic decay of the W:

$$e^+p \to e^+W^\pm X, \;\; W^\pm \to e^\pm\nu_e(\overline{\nu}_e), \;\; W^\pm \to \mu^\pm\nu_\mu(\overline{\nu}_\mu)$$

In only one of these events (shown in Figure 5.10) also the scattered positron is observed, which allows to calculate the invariant mass of the (μ,ν) pair to $M_{\mu\nu} = 83^{+15}_{-10}$ GeV, i. e. consistent with M_W. Since W's are mainly photoproduced with a radiation of a W from the quark line and a total cross section of 70 fb per channel and charge, the other three events all lie at the edge of the phase space, are very unlikely to result from this process, and hence yet unexplained.

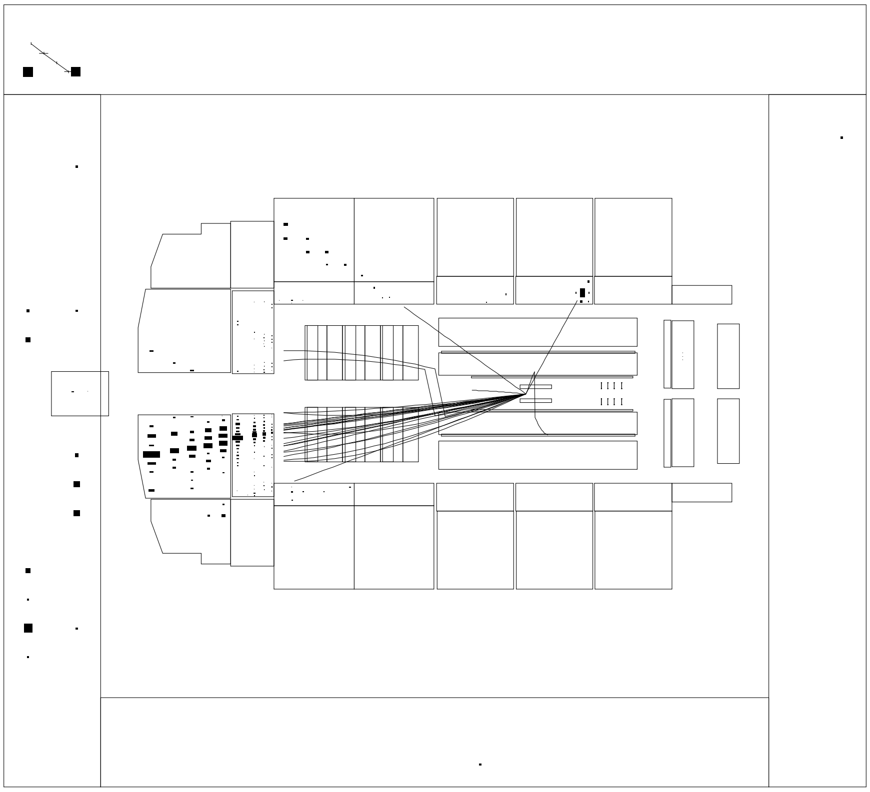

Figure 5.10: One of the six events observed with an isolated e^- oder $\mu^\pm$ of high transverse momentum in the e^+p sample with an imbalance in transverse momentum. This event is consistent with the hypothesis $e^+p \to e^+W^-X$; $W^- \to \mu^-\bar{\nu}$. Upper left track: μ^-, upper right track: e^+, lower left tracks: hadronic jet [5].

5.4.2 Photo- and electroproduction of charm quarks

Heavy flavours in the hadronic final state, like jets, carry a lot of information about the dynamics of the unobservable quarks and gluons. They thus provide access to the underlying hard partonic processes of high energy ep interactions. The aim is to test the description of the production processes by perturbative QCD, and to extract information on the parton distributions of the initial state hadron. In the conventional picture of ep scattering, charm is produced almost exclusively via boson gluon fusion and thus directly probes the gluon content of the proton.

Open charm at HERA has mainly been reconstructed in the fragmentation and decay chain $c \to D^{*+} \to D^0\pi^+ \to (K^-\pi^+)\pi^+$ exploiting the clean experimental signal in the mass difference distribution of $\Delta m = m(K^-\pi^+\pi^+) - m(K^-\pi^+)$ (and similar for the charge conjugate).

It is possible to make use of the kinematic information from the reconstructed charm tag, in order to reconstruct the momentum fraction x_g of the incoming gluon and thus arrive at a direct measurement of the density function $g(x_g)$. We have shown a first measurement [20] of the differential charm cross section as a function of x_g^{OBS}, which was reconstructed from the D^* meson and the scattered positron (Figure 5.11). The analysis of the three times larger 1996 sample is underway. QCD predictions in next-to-leading order (NLO) for such

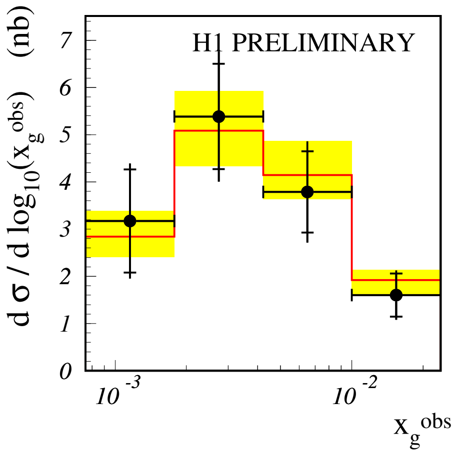

Figure 5.11: Differential charm cross section $\sigma(ep \rightarrow eD^{*}X)$, for $Q^2 > 2$ (GeV/c)^2. as function of the parton momentum fraction x_g^{OBS}, reconstructed from the D^* meson and the scattered electron. The H1 data are shown as points with error bars, the QCD calculations in NLO using the GRV94 HO parton distribution set is shown as solid histogram. The shaded band represents the variation of the cross section due to the variation of the mass of the charm quark between 1.3 and 1.7 GeV/c^2.

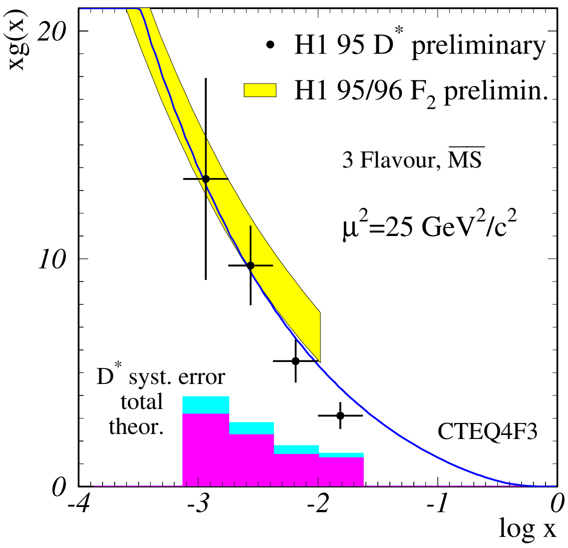

Figure 5.12: Gluon density $x_g g(x_g)$ as function of x_g extracted from the charm production cross section (data points with statistical errors) compared to the result of the H1 QCD analysis of the inclusive F_2 measurement at $\mu^2 = 4m_c^2 + \overline{Q^2} = 24$ GeV^2 (light shaded band). The solid line is the theoretical prediction from the CTEQ4F3 parameterization at this scale (μ^2).

distributions at the level of observable hadrons have recently become available [25]

The programs have been adapted to the H1 analysis, results are also shown in Figure 5.11 (Thesis D. Müller). The QCD program also yields the correlations with the 'true' x_g which can be used to unfold the gluon density from the measured spectrum. The result of such an unfolding procedure is shown in Figure 5.12. There is good agreement with the standard method to extract gluon densities, the QCD analysis of the inclusive structure function F_2, with our method for those data points where the kinematics overlap. This represents a non-trivial confirmation of the applied QCD concepts and of the universality of the parton distributions.

Measurements of differential charm production cross sections are being pursued also in the photoproduction regime (Thesis M. zur Nedden), using a data sample four times as large as the 1994 set that provided the basis of our first publication in this area [24]. There exist several theoretical approaches within perturbative QCD to describe the process, where charm quarks may or may not play a role as active partons in the initial state proton and photon (which can fluctuate into a hadronic state as well). With the increased statistics, it should become possible to identify the kinematic range where these concepts are appropriate and may be used to extract information about parton densities.

Particular interest at HERA has been created by a fraction of about 10% of the DIS events which exhibit the characteristics of a diffractive interaction: the hadronic system recoiling against the scattered electron is separated from the beam axis by a region void of any particle

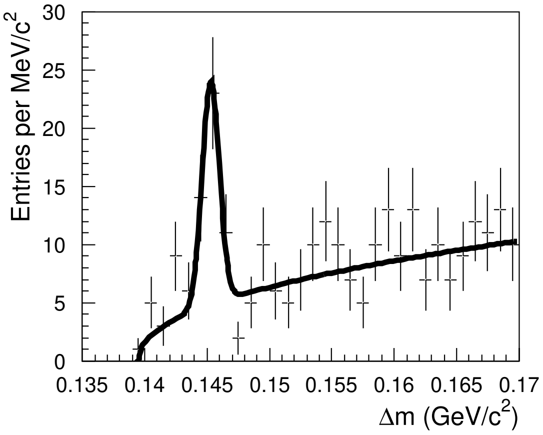

Figure 5.13: The mass difference distribution for $D^{*\pm}$ candidates in diffractive DIS events with no energy deposition in the calorimeter more forward than at pseudo-rapidity $\eta_{max} = 3.2$. The solid line is a Gaussian plus polynomial fit used to extract the signal.

flow. These processes are interpreted as exchange of a color-less object. Charm production holds the promise of providing important keys to the theoretical understanding of diffraction; some kinematic distributions are remarkably sensitive to the dynamics of the underlying exchange [26]. D^* signals in diffractive ep interactions have been reported [19, 24], albeit with very poor statistics. With the integrated luminosity collected in 1997, it will become possible to investigate the phenomenon in detail. The signal obtained from the 1995, 1996 and part of the 1997 data, requiring the most forward energy deposition in the calorimeter and forward detectors to have pseudo-rapidity $\eta_{max} < 3.2$ is shown in Figure 5.13 (Thesis S. Hengstmann). Here the kinematic region is $Q^2 > 2$ GeV/c^2, $p_\perp(D^*) > 1.5$ GeV/c and $x_{\mathbb{P}} < 0.005$, where $x_{\mathbb{P}}$ denotes the momentum fraction of the exchanged object – generically termed 'Pomeron' – in the proton.

References

[1] Observation of Events at very High Q^2 in ep collisions at HERA, C. Adloff et al., Z. Phys. **C74** (1997), 191 - 205.

[2] A Measurement of the Proton Structure Function $F_2(x, Q^2)$ at Low x and Low Q^2 at HERA, C. Adloff et al., Nucl. Phys. **B497** (1997), 3 - 30.

[3] P. Bruel, High Q^2 DIS results and search for leptoquarks at HERA, XXIII. Rencontres de Moriond, on Electroweak Interactions and Unified Theories, Les Arcs, France, March 1998; available at *http://www-h1.desy.de/h1/www/publications/hiq2/hiq2.html.*

[4] G. Bernardi, New H1 results at high Q^2, talk given at DESY, Hamburg (March 1998); available at *http://www-h1.desy.de/h1/www/publications/hiq2/hiq2.html.*

[5] Observation of Events with an Isolated High Energy Lepton and Missing Transverse Momentum at HERA, C. Adloff et al., to be submitted to Phys. Lett.

[6] Photoproduction of $\bar{K}^0$ and Λ at HERA and a Comparison to Deep Inelastic Scattering, C. Adloff et al., Z. Phys. **C76** (1997), 213 - 221.

[7] Low Q^2 Jet Production at HERA and Virtual Photon Structure, C. Adloff et al., Phys. Lett. **B415** (1997), 418 - 434.

[8] Measurement of the Inclusive Di-Jet Cross Section in Photoproduction and Determination of an Effective Parton Distribution in the Photon, C. Adloff et al., Eur. Phys. J. **C1** (1998), 97 -107.

[9] Photoproduction of $\Psi(2s)$ Mesons at HERA, C. Adloff et al., Phys. Lett. **B** (1997), in print.

[10] Inclusive Measurement of Diffractive Deep-Inelastic ep Scattering, C. Adloff et al., Z. Phys. **C76** (1997), 613 - 629.

[11] Thrust Jet Analysis in Deep-Inelastic Large-Rapidity-Gap Events, C. Adloff et al., Eur. Phys. J. **C1** (1998), 495 - 507.

[12] Diffraction Dissociation in Photoproduction at HERA, C. Adloff et al., Z. Phys. **C74** (1997), 221 - 235.

[13] Bose-Einstein Correlations in Deep Inelastic ep Scattering at HERA, C. Adloff et al., Z. Phys. **C75** (1997), 437 - 451.

[14] Proton Dissociative ρ and Elastic Φ Electroproduction at HERA, C. Adloff et al., Z. Phys. **C75** (1997), 607 - 618.

[15] Measurement of Event Shape Variables in Deep Inelastic ep Scattering, C. Adloff et al., Phys. Lett. **B406** (1997), 256 - 270.

[16] Evolution of ep Fragmentation and Multiplicity Distributions in the Breit Frame, C. Adloff et al., Nucl. Phys. **B504** (1997), 3 - 23.

[17] Measurement of the Gluon Density in the Proton, Thesis D. Müller (1998).

[18] Heavy quark and jet production by real and virtual photons, F. Sefkow, Proc. 17. Int. Conf. on Physics in Collision, Bristol, England (1997), in print.

[19] A Measurement of the Production of $D^{*\pm}$ Mesons in Deep–Inelastic Diffractive Interactions at HERA, H1 Collaboration, contr. No. pa02-060, Int. Conf. on High Energy Physics, July 1996, Warsaw, Poland.

[20] Determination of the gluon density in the proton from deep inelastic ep charm production using NLO QCD, H1 Collaboration, contr. No. 275 at Int. Europhysics Conf. on High Energy Physics, August 1997, Jerusalem, Israel.

[21] Improving the z-Vertex Trigger, D. Müller und F. Sefkow, H1 note H1-04/98-539, April 1998.

[22] ep physics beyond 1999, H1-collaboration, H1 note H1-10/97-531, November 1997.

[23] H1 high luminosity upgrade 2000, CIP and level 1 vertex trigger, M. Cuje et al., H1 note H1-01/98-535, January 1998.

[24] Photoproduction of $D^{*\pm}$ Mesons in Electron - Proton Collisions at HERA, S. Aid et al., Nucl. Phys. **B472** (1996), 32.

[25] B. W. Harris and J. Smith, Nucl. Phys. **B452** (1995), 109; Phys. Lett. **B353** (1995), 535.

[26] W. Buchmüller, M.F. McDermott and A. Hebecker, Phys. Lett. **B404** (1997), 353.